A Structural Basis for the Regulation of an H-NOX-Associated Cyclic-di-GMP Synthase/Phosphodiesterase Enzyme by Nitric Oxide-Bound H-NOX

Tanaya Lahiri,[†] Bowu Luan,[†] Daniel P. Raleigh,[†,§,‡] and Elizabeth M. Boon*[,†,§,‡]

[†]Department of Chemistry, Stony Brook University, Stony Brook, New York 11794-3400, United States
[‡]Institute of Chemical Biology and Drug Discovery, Stony Brook University, Stony Brook, New York 11794-3400, United States
[§]Graduate Program in Biochemistry and Structural Biology, Stony Brook University, Stony Brook, New York 11794-3400, United States

S *Supporting Information*

ABSTRACT: Biofilms are surface-attached communities of bacteria enclosed in a polysaccharide matrix. Bacteria in a biofilm are extremely resistant to antibiotics. Several recent reports have linked the signaling molecule nitric oxide (NO) with biofilm dispersal. We have previously reported that an H-NOX (heme-nitric oxide/oxygen binding) protein in the biofilm-dwelling bacterium *Shewanella woodyi* mediates NO-induced biofilm dispersal. In *S. woodyi*, H-NOX (*Sw*H-NOX) is cocistronic with a gene encoding a dual-functioning diguanylate cyclase/phosphodiesterase enzyme, designated here as HaCE (H-NOX-associated cyclic-di-GMP processing enzyme). Enzymes such as these are responsible for regulating the intracellular concentrations of cyclic-di-GMP, a secondary signaling molecule essential to biofilm formation in bacteria. We have demonstrated that NO-bound *Sw*H-NOX regulates both enzymatic activities of *Sw*HaCE, resulting in decreased cellular cyclic-di-GMP levels and disruption of biofilm formation. Thus, H-NOX/HaCE represents a potential drug target for regulating biofilm formation. In this work, the *Sw*H-NOX surface residues critical for the formation of a protein complex with *Sw*HaCE are identified using nuclear magnetic resonance, fluorescence quenching, and cosedimentation. Enzyme assays confirm this protein−protein interface and its importance for H-NOX/HaCE function.

Surface mutations in the N-terminal helices of H-NOX abrogate binding and regulation of a cyclic-di-GMP synthase/phosphodiesterase.
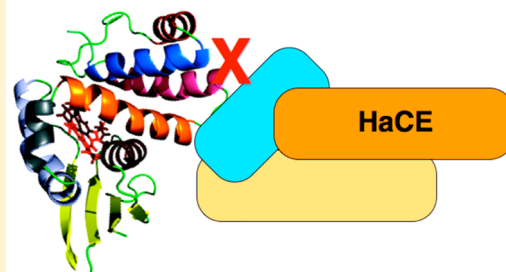
B iofilm formation is an important phenotype in bacteria, where cells switch from a motile, free-swimming, single-cell growth mode to a surface-attached, sessile, community of cells encapsulated in a matrix consisting of exopolysaccharide, protein, and DNA.[1,2] Bacteria within biofilms are extremely resistant to antibiotics and are thought to be responsible for several drug-resistant infectious diseases. Biofilm development is poorly understood in general, but the intracellular concentration of bis-(3′−5′)-cyclic dimeric guanosine monophosphate (cyclic-di-GMP or c-di-GMP) has been shown to be important for the regulation of motility and biofilm formation,[3,4] in addition to many other important signaling processes, including cell division, transcriptional regulation, and virulence.[5−8]

In bacteria, two classes of enzymes maintain the intracellular pool of cyclic-di-GMP. Cyclic-di-GMP is synthesized from two molecules of GTP by GGDEF domain-containing diguanylate cyclases (DGCs).[9−11] Cyclic-di-GMP is hydrolyzed by ExL domain-containing phosphodiesterases (PDEs)[12−14] to form the linear metabolite 5′-phosphoguanylyl-(3′→5′)-guanosine (pGpG). Because cyclic-di-GMP signaling and bacterial biofilms are central to many infectious diseases, the pathways

that contribute to the regulation of intracellular cyclic-di-GMP concentrations are potentially important antibiotic drug targets.

Nitric oxide (NO) is a well-established and important signaling molecule in mammals that regulates a variety of physiological processes, including vasodilation and neurotransmission.[15] The enzyme soluble guanylate cyclase (sGC) acts as an NO sensor via its N-terminal heme-nitric oxide/oxygen binding domain.[16] Interestingly, several different groups have recently observed that low concentrations of NO induce biofilm dispersal in a variety of bacterial species.[17−19] In bacteria, H-NOX domains typically exist as stand-alone proteins that regulate cocistronic histidine kinase [H-NOX-associated histidine kinase (HahK)] or c-di-GMP synthase and/or phosphodiesterase [H-NOX-associated cyclic-di-GMP processing enzyme (HaCE)] proteins.[20,21] In general, the biophysical characterization of these H-NOX/enzyme complexes is lacking.

H-NOX signaling in *Legionella pneumophila* and *Shewanella woodyi*, both of which encode a diguanylate cyclase/

phosphodiesterase protein in the same operon as an H-NOX domain, has been characterized.[22] It is reported that the H-NOX-associated protein Lpg1057 (*Lp*HaCE) from *L. pneumophila* has *in vitro* diguanylate cyclase activity that is inhibited by NO-bound H-NOX.[23] The phosphodiesterase domain was found to be inactive. In *S. woodyi*, H-NOX regulates the DGC and PDE activities of *Sw*HaCE (Swoo_2750), previously termed *Sw*DGC.[24] In the absence of NO, *Sw*H-NOX stimulates diguanylate cyclase activity while the phosphodiesterase activity remains at basal levels. In the presence of NO-bound H-NOX, however, this pattern is reversed. *Sw*HaCE displays basal level cyclase activity, whereas the phosphodiesterase activity is upregulated. These results underlie the additional finding that nanomolar NO leads to less biofilm and a decreased level of cyclic-di-GMP in *S. woodyi*. These data are consistent with H-NOX acting as an NO sensor that regulates biofilm formation by modulating the intracellular level of cyclic-di-GMP in bacteria.

Therefore, the H-NOX/HaCE protein−protein interaction is important for regulating the biofilm formation pathway in some bacteria. Here we use a combination of techniques to study how HaCE proteins are regulated by H-NOX. We employ NMR chemical shift perturbation experiments to identify the residues of *Sw*H-NOX that interact with *Sw*HaCE. The role of these residues was confirmed by enzyme activity assays as well as fluorescence binding studies with mutant proteins. Sedimentation equilibrium studies were used to assess the stoichiometry of the *Sw*H-NOX/*Sw*HaCE complex. The data were used to generate a model for H-NOX regulation of HaCE activity.

■ EXPERIMENTAL PROCEDURES

Materials and General Methods. All reagents were obtained at their highest available purity and used as received. All enzymes were purchased from New England Biolabs.

Protein Expression and Purification. *Sw*H-NOX and *Sw*HaCE were expressed and purified as described previously.[22,24] In brief, the plasmid containing the *Sw*H-NOX gene was transformed into *Escherichia coli* Tuner(DE3)pLysS cells for protein expression. The cells were grown in yeast extract medium containing a final sodium phosphate concentration of 100 mM. The protein expression was induced with 10 μM IPTG (final concentration) at 18 °C overnight. The pellet was harvested and stored at −80 °C until it was purified. For purification, the pellet was thawed on ice and resuspended in H-NOX A buffer [50 mM sodium phosphate and 300 mM sodium chloride (NaCl) (pH 8.0)]. After sonication, the lysate was spun at 18000 rpm (39200g) for 1 h. The cleared supernatant was loaded on a nickel-NTA (GE) column, and the protein was eluted using an imidazole gradient of H-NOX B buffer [50 mM sodium phosphate, 300 mM NaCl, and 250 mM imidazole (pH 8.0)]. The plasmid encoding *Sw*HaCE[24] was transformed into *E. coli* BL21(DE3)pLysS cells for protein expression. The cells were grown in 2XYT medium containing 16 g of tryptone, 10 g of yeast extract, and 5 g of NaCl per liter. Protein expression was induced with 100 μM IPTG (final concentration) at 16 °C overnight. The pellet was resuspended in lysis buffer containing 50 mM Tris base, 10 mM magnesium chloride (MgCl$_2$), 25 mM potassium chloride (KCl), 300 mM NaCl, 10% glycerol, and 2 mM βME (β-mercaptoethanol) (pH 8.0). Phenylmethanesulfonyl fluoride (PMSF) dissolved in methanol was added to a final concentration of 1 mM to the resuspended pellet prior to lysis to inhibit protease activity. After sonication, the lysate was spun at 18500 rpm (41400g) for 1 h. The cleared supernatant was loaded on a nickel-NTA column (GE), and the protein was eluted using an imidazole gradient in lysis buffer. After elution off the Ni column, the protein was loaded on Superdex-200 (GE) equilibrated in lysis buffer without glycerol and PMSF to obtain >95% pure protein.

To produce ^{13}C- and ^{15}N-labeled protein, *E. coli* Tuner-(DE3)pLysS cells transformed with the *Sw*H-NOX plasmid were grown in M9 minimal medium supplemented with ^{15}NH$_4$Cl and ^{13}C-labeled glucose (Cambridge Isotope Laboratories, Inc.) as the sole sources of ^{15}N and ^{13}C, respectively. Protein expression was induced by adding 10 μM IPTG (final concentration) at 25 °C and allowing cultures to grow overnight. Then the protein was purified by nickel-NTA affinity chromatography followed by gel filtration using Superdex 200. The yield of the isotope-labeled protein was ∼10 mg/L. For all protein-based assays described below, the protein concentrations were determined using the Bradford Protein Assay (Thermo Scientific, Pierce).[25] The standard curve for the assay was prepared using BSA (Thermo Scientific, Pierce).

Site-Directed Mutagenesis. The Stratagene QuikChange protocol was used to introduce several *Sw*H-NOX point mutations. The following complementary primers were used to make the E16K, F17A, and E20K *Sw*H-NOX mutants: E16K, 5′-GGAG TTG ATT GAA GAT AAA TTC GGA TAT GAA ACC-3′; F17A, 5′-GAG TTG ATT GAA GAT GAG GCT GGA TAT GAA ACC-3′; and E20K, 5′-GAG TTC GGA TAT AAA ACC TTA GAT ACT TTA CTT G-3′ (the underlined portions are the mutated codons). Phusion polymerase was purchased from New England Biolabs. The mutagenesis products were transformed into *E. coli* Dh5α cells for propagation. The mutations were confirmed using DNA sequencing results obtained from the DNA sequencing facility at Stony Brook University. The expression and purification of *Sw*H-NOX surface mutants were conducted using the same protocols as described above for the wild-type *Sw*H-NOX protein.

NMR and Data Analysis. The *Sw*H-NOX Fe(II)−CO complex was used in the NMR studies to avoid paramagnetic effects resulting from the unpaired electron in the Fe(II)−NO and Fe(II)−unligated *Sw*H-NOX complexes. The Fe(II)−CO complex was prepared in an anaerobic glovebag as previously described.[26] The *Sw*H-NOX concentration was 400 μM, dissolved in 50 mM sodium phosphate, 50 mM NaCl, and 10 mM sodium dithionite (pH 7.6). Triple-resonance NMR experiments for the backbone assignments of *Sw*H-NOX (HNCO, HNCACB, CBCACONH, and HNCA) were performed at 25 °C on a Bruker 900 MHz spectrometer equipped with a cryoprobe at the New York Structural Biology Center (New York, NY). Data were processed using NMRPipe[27] followed by analysis using Sparky;[28] 75% of the backbone resonances were assigned.

Transverse relaxation-optimized spectroscopy (TROSY)-edited ^{15}N−^{1}H HSQC experiments were performed on the same spectrometer at 25 °C for the following samples: (1) the ^{15}N-labeled Fe(II)−CO *Sw*H-NOX complex and (2) the ^{15}N-labeled Fe(II)−CO *Sw*H-NOX complex and the nonisotopically labeled binding partner *Sw*HaCE, at a ratio of 1:1.25. The buffer used was the same as that used in the three-dimensional (3D) NMR experiments. Then, the weighted average chemical shift difference (Δ in parts per million) was calculated using the equation

$$\Delta\delta = \{[(\Delta H)^2 + (\Delta N/5)^2]/2\}^{1/2} \qquad (1)$$

Tryptophan Fluorescence Quenching. Intrinsic fluorescence experiments were conducted on a PTI spectrofluorometer. *Sw*HaCE (1 μM) was placed in a cuvette, and the *Sw*H-NOX Fe(II)−NO complex (WT and mutants E16K, F17A, and E20K, separately) was titrated serially into the protein while being stirred constantly at 25 °C. *Sw*HaCE was diluted to 10% of the starting volume (2000 μL). Titration was continued until the maximal change in fluorescence had been achieved. The data were fit to a first-order binding equation in Origin:

$$temp = (P + x + K_d)^2 - 4Px; \ y$$
$$= A_1(P + x + K_d - temp^{1/2})/P/2 \qquad (2)$$

Sedimentation Velocity and Sedimentation Equilibrium. Experiments were conducted at 4 °C on a Beckman Optima XL-Analytical ultracentrifuge using an An-60 Ti rotor. For sedimentation velocity experiments, *Sw*HaCE was incubated with the *Sw*H-NOX Fe(II)−NO complex (WT and mutant E16K, separately), and the protein complex was centrifuged at 50000 rpm (201240g) for 24 h with 60 scans at 280 nm. The protein concentration was adjusted so that the absorbance was 0.8 at 280 nm. The data were analyzed using SEDFIT.[29] The buffer consisted of 50 mM Tris-HCl, 250 mM NaCl, 25 mM KCl, 10 mM MgCl$_2$, and 2 mM βME (pH 8.0).

For the equilibrium experiments with *Sw*HaCE alone, *Sw*HaCE was analyzed at three rotor speeds (9000, 14000, and 18000 rpm, which are equal to 6500g, 15800g, and 26100g, respectively), which were calculated using the molecular mass of *Sw*HaCE (74.5 kDa). Two scans were collected at the end of each speed. The protein absorbance was followed at 280 and 260 nm. The data were analyzed using HeteroAnalysis (University of Connecticut Analytical Ultracentrifugation Facility) to determine the molecular mass for *Sw*HaCE alone in solution. The data were fit globally across samples and speeds to yield the apparent molar mass.

For the equilibrium experiments with the *Sw*H-NOX/*Sw*HaCE complex, *Sw*HaCE, either the WT or the E16K mutant, was incubated with WT *Sw*H-NOX, as either the Fe(II)-unligated or *Sw*H-NOX Fe(II)−NO complex, in 1:1, 1:2, and 1:5 molar ratios, and analyzed at three rotor speeds (9000, 14000, and 18000 rpm, which are equal to 6500g, 15800g, and 26100g, respectively) with two scans at the end of each speed. The scans were collected at an absorbance of 400 nm for experiments with the Fe(II)−NO complex or 430 nm for experiments with the Fe(II)-unligated complex to follow the heme absorbance of *Sw*H-NOX. The protein concentration was adjusted so that the absorbance was 0.5 at 430 nm. For the equilibrium experiments with *Sw*H-NOX alone, *Sw*H-NOX was analyzed at three rotor speeds (17000, 27000, and 34000 rpm, which are equal to 23300g, 58700g, and 93000g, respectively), which were calculated using the molecular mass of *Sw*H-NOX (22.5 kDa).

Enzyme Activity Measurements Using the Malachite Green Assay. The SensoLyte MG phosphate assay kit was purchased from AnaSpec. For the diguanylate cyclase enzyme assays, *Sw*HaCE by itself (1 μM), or in the presence of the *Sw*H-NOX Fe(II)-unligated complex (WT, E16K, F17A, or E20K in a 1:20 concentration ratio), was incubated on ice for 10 min to allow the proteins to form a complex. The protein mixtures (20 μL) were then added to 180 μL a prepared solution containing 200 μM GTP (substrate), 5 mM MgCl$_2$,

and 1× buffer [50 mM Tris base and 10 mM MgCl$_2$ (pH 7.5)]. The reaction mixture was incubated for 10 min at 25 °C followed by boiling at 100 °C to quench the reaction. After being cooled, the mixture was spun at 14000 rpm (16900g) for 5 min to remove any precipitate; 70 μL of the supernatant was mixed with 10 μL of 3 units/mL IPP [inorganic pyrophosphatase (NEB)] in a 96-well plate and incubated at 25 °C for 10 min to hydrolyze the inorganic pyrophosphate (PP$_i$) produced during the reaction. Then, 20 μL of Malachite green reagent was added and the solution mixed, and the plate was read at 610 nm using a Perkin-Elmer Viktor X5 microplate reader. The absorbance readings were corrected for protein only and GTP only background. This experiment measured the initial velocity for the diguanylate cyclase activity for *Sw*HaCE and *Sw*HaCE in complex with *Sw*H-NOX. This experiment was repeated in at least three fully independent experiments.

NO Dissociation Kinetics. NO dissociation kinetics of *Sw*H-NOX mutants E16K, F17A, and E20K were conducted as previously described.[30]

■ RESULTS

Despite the importance of biofilms in infectious diseases, the mechanisms that regulate biofilm formation and dispersal are poorly understood. In this study, we have characterized the H-NOX/HaCE protein complex from *S. woodyi* to improve our understanding of how NO causes biofilm dispersal in this bacterium.

Chemical Shift Perturbation Assays Reveal the Binding Interface for *Sw*HaCE. We collected HNCO, HNCACB, CBCACONH, and HNCA spectra to assign the backbone resonances of *Sw*H-NOX. Using standard methods, resonances from 75% of the *Sw*H-NOX residues (∼140 residues) could be assigned, and these assignments were used to probe the binding of *Sw*HaCE (Figure 1). HSQC NMR spectra of the ¹⁵N-labeled *Sw*H-NOX Fe(II)−CO complex were compared to the spectra of the 1:1.25 complex of the ¹⁵N-labeled *Sw*H-NOX Fe(II)−CO complex in the presence of *Sw*HaCE. In the presence of *Sw*HaCE, there was a significant loss of signal in the *Sw*H-NOX HSQC spectrum because of peak broadening, presumably
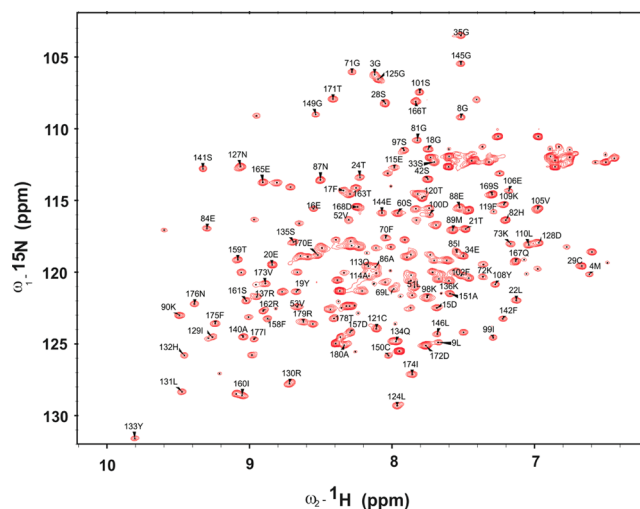

Figure 1. Backbone assignment for *Sw*H-NOX [as the Fe(II)−CO complex]. Approximately 75% of the peaks were assigned using extensive 3D experiments. The x-axis represents the chemical shift in ¹H, and the y-axis represents the chemical shift in ¹⁵N.

because the total size of the *Sw*H-NOX/*Sw*HaCE complex is expected to be at least 100 kDa (74.5 kDa for *Sw*HaCE and 22.5 kDa for *Sw*H-NOX). Hence, TROSY spectra were recorded for *Sw*H-NOX alone (Figure 2, red) and in complex
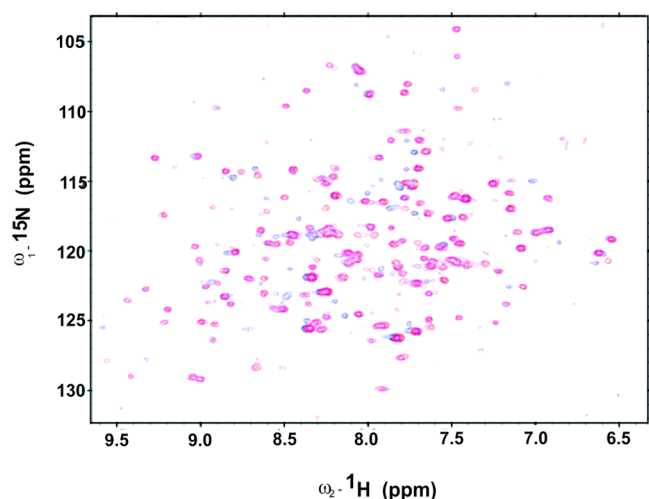

Figure 2. Chemical shift mapping for *Sw*HaCE and *Sw*H-NOX complex formation. The $^{15}N-^{1}H$ HSQC spectrum (red) was recorded for a sample containing uniformly ^{15}N-labeled 50 μM *Sw*H-NOX [as the Fe(II)−CO complex]. The blue spectrum was recorded for a 1:1.25 ratio of ^{15}N-labeled *Sw*H-NOX [as the Fe(II)−CO complex] to unlabeled *Sw*HaCE. An overlay of these spectra indicates that peaks for some residues are shifted, indicating a change in their chemical environment in the presence of *Sw*HaCE.

with *Sw*HaCE (Figure 2, blue). No line broadening effects were observed, and the TROSY spectrum for the complex showed only one set of peaks, indicating fast exchange on the NMR time scale.

The chemical shifts of some residues shifted significantly for the protein/protein complex (Figure 2, blue), compared to the spectrum of *Sw*H-NOX alone (Figure 2, red). To correlate the changes in chemical shift with structure, a homology model of *Sw*H-NOX was generated (Figure 3A). The change in chemical shift for each assigned residue of *Sw*H-NOX (with and without *Sw*HaCE) was plotted (Figure 3B). Assuming a ratio of 0.02 to be a significant change, there are ∼11 *Sw*H-NOX residues that shift upon exposure to *Sw*HaCE.

We were particularly interested in a set of five residues (amino acids 16−20) in the N-terminal helices of *Sw*H-NOX that displayed the maximal shift. These residues form a cluster in N-terminal helices αB and αC on the surface of *Sw*H-NOX, suggesting this contributes to the binding site for *Sw*HaCE. To test this hypothesis, we constructed three *Sw*H-NOX point mutants (highlighted in Figure 4), E16K, E20K, and F17A. We reasoned that charge reversal mutants (E16K and E20K) would be expected to significantly perturb binding if these residues play a key role and that reducing the bulk of F17 might weaken hydrophobic interactions during binding.

Characterization of ligand binding (binding of CO and NO to ferrous *Sw*H-NOX and binding of CN^{-} to ferric *Sw*H-NOX) and NO dissociation kinetics were conducted for the WT and the surface mutants of *Sw*H-NOX. The Soret values and k_{off}(NO) calculated for H-NOX surface mutants were similar to those of WT H-NOX (Table S1 of the Supporting Information), confirming that mutating these surface residues
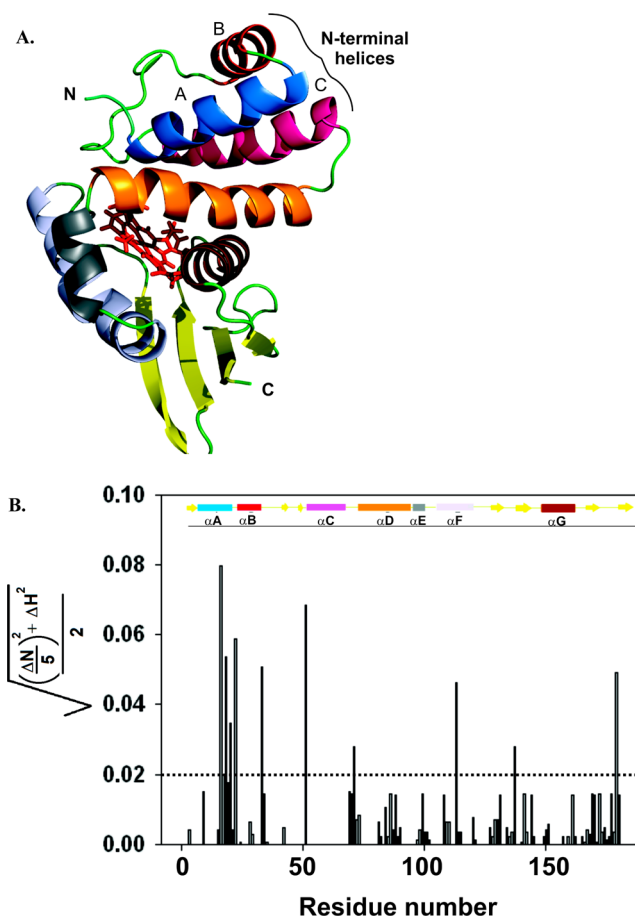

Figure 3. (A) Ribbon structure of the *Sw*H-NOX protein from *S. woodyi*. This figure is a homology model generated in PyMOL using the solution-state NMR structure of *Shewanella oneidensis*[26] (So2144, Protein Data Bank entry 2KII, chain A). The heme is shown as red sticks. The N- and C-termini of the protein are denoted. The seven different helices are depicted in different colors: blue for helix αA, red for helix αB, hot pink for helix αC, orange for helix αD, gray for helix αE, purple for helix αF, and chocolate brown for helix αG. (B) Chemical shift changes for *Sw*H-NOX upon addition of *Sw*HaCE. The shifts (*Sw*H-NOX to *Sw*H-NOX/*Sw*HaCE), calculated as $\{[(\Delta N/5)^2 + (\Delta H)^2]/2\}^{1/2}$, are plotted against the primary sequence residue number. The cutoff shift was kept at 0.02, and shifts above 0.02 (dashed line) were considered significant. The secondary structure of *Sw*H-NOX is shown as a cartoon in which the rectangles represent α-helices and the solid arrows represent β-strands. The color code corresponds to the ribbon diagram in panel A.

does not affect the overall structure or heme properties of the *Sw*H-NOX protein.

Fluorescence Quenching Assays Indicate That Binding of *Sw*HaCE Is Significantly Weaker for Surface Mutants E16K, F17A, and E20K Than for WT *Sw*H-NOX. *Sw*HaCE has seven Trp residues, while *Sw*H-NOX has none; thus, we reasoned that binding of *Sw*H-NOX to *Sw*HaCE might perturb the Trp fluorescence intensity of *Sw*HaCE. Therefore, the steady-state fluorescence of 1 μM *Sw*HaCE was followed at 370 nm in the presence of increasing concentrations of NO-bound H-NOX to assess *Sw*H-NOX/*Sw*HaCE binding. The *Sw*H-NOX Fe(II)−NO complex (WT or mutant, separately; ∼1−10 μM) was titrated into the *Sw*HaCE solution while it was being stirred constantly until the maximal change in fluorescence had been achieved. We observed a quenching of the fluorescence signal as a function of an increasing
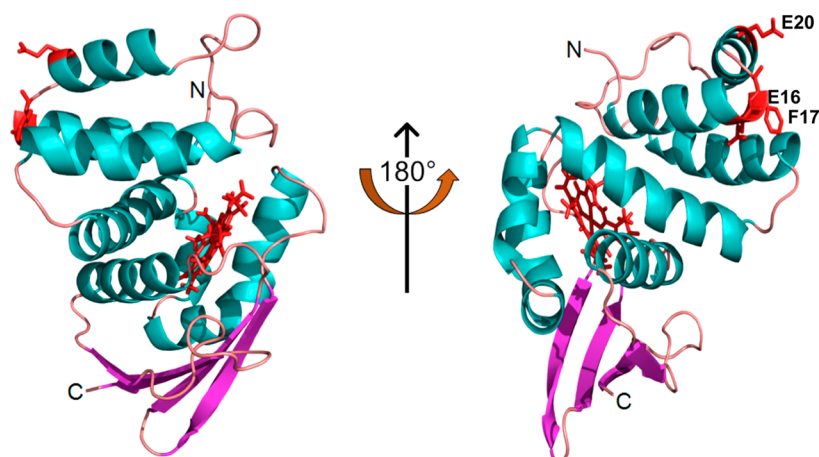
Figure 4. *Sw*H-NOX surface residues identified from chemical shift mapping. The *Sw*H-NOX residues with the maximal perturbation (E16, F17, and E20) upon incubation with *Sw*HaCE are colored red. The heme cofactor is also colored red. These residues likely represent the binding patch for *Sw*HaCE.

concentration of the *Sw*H-NOX Fe(II)−NO complex in solution (Figure 5). Here, to have positive numbers, the
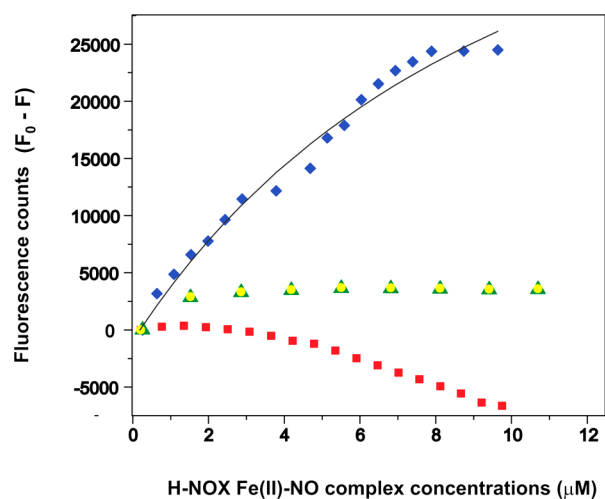

Figure 5. Tryptophan fluorescence quenching experiments for assessing *Sw*H-NOX/*Sw*HaCE binding. The Fe(II)−NO complex of *Sw*H-NOX [WT (blue diamonds), E16K (red squares), F17A (green triangles), and E20K (yellow circles)] was titrated into a *Sw*HaCE solution (1 μM) to determine the amount of *Sw*HaCE Trp quenching. The difference in fluorescence $(F_0 − F)$ with and without *Sw*H-NOX is plotted as a function of *Sw*H-NOX Fe(II)−NO complex concentration. WT *Sw*H-NOX caused significant quenching of *Sw*HaCE fluorescence. In general, the *Sw*H-NOX mutants do not quench *Sw*HaCE fluorescence, indicating a loss of binding. From these data, the apparent equilibrium dissociation constant for the *Sw*H-NOX/*Sw*HaCE complex was determined to be ∼2.5 μM (the gray line shows the fit used to determine $K_{D,app}$). Each titration was conducted in triplicate.

difference $(F_0 − F)$ is plotted as a function of the concentration of NO-bound H-NOX in solution for each *Sw*H-NOX construct. The data were corrected for dilution and inner filter effects and plotted against *Sw*H-NOX Fe(II)−NO complex concentration. The apparent dissociation constant $(K_{D,app})$ for the complex was determined to be 2.5−3 μM from three independent runs. This likely overestimates the true K_D, as the concentrations used were high and not under pseudo-first-order conditions, to account for the sensitivity of the detector.

Nonetheless, the effect of *Sw*H-NOX surface mutations on binding to *Sw*HaCE could be easily determined in this assay.

For the titrations with the Fe(II)−NO complex of the E16K mutant of *Sw*H-NOX, the fluorescence signal for *Sw*HaCE did not decrease over time and actually increased slightly (Figure 5). This indicates that the E16K mutation abolished binding of *Sw*H-NOX to *Sw*HaCE. The slight increase in the magnitude of the fluorescence signal toward the end of the titration could be due to conformational changes resulting from interactions of the *Sw*H-NOX E16K mutant with other regions of *Sw*HaCE at high H-NOX concentrations. For the *Sw*H-NOX F17A and E20K mutants, we observed significantly less quenching of the *Sw*HaCE signal than for the WT, suggesting a reduced binding affinity for each of these mutants for *Sw*HaCE (Figure 5). These results confirm that surface residues E16, F17, and E20 in N-terminal helices αB and αC of *Sw*H-NOX each contribute to *Sw*HaCE binding and likely are part of a binding surface for interaction with *Sw*HaCE.

Sedimentation Equilibrium Indicates That *Sw*HaCE Forms a Dimer in Solution and the *Sw*H-NOX/*Sw*HaCE Complex Forms a Heterotetramer. On the basis of the NMR and fluorescence titration experiments described above, we concluded that *Sw*H-NOX and *Sw*HaCE form a protein/protein complex. We used sedimentation equilibrium measurements to determine the stoichiometry of this complex. Sedimentation equilibrium experiments are extensively used to determine the molecular masses of proteins and protein complexes in solution.[31] On the basis of previously characterized diguanylate cyclases, it is expected that active diguanylate cyclases exist as dimers in solution.[32−34] Because *Sw*HaCE is an active cyclase enzyme,[24] we wanted to determine if *Sw*HaCE also forms oligomers (dimers) in solution, and we wanted to determine if the oligomerization state changes upon formation of a complex with *Sw*H-NOX.

Sedimentation equilibrium experiments were conducted with *Sw*HaCE alone, *Sw*H-NOX [as the Fe(II)−NO or Fe(II)-unligated complex, separately] alone, and a mixture of *Sw*HaCE and *Sw*H-NOX [as the Fe(II)−NO or Fe(II)-unligated complex, separately] at a ratio of 1:1.5. These data are summarized in Table 1. For *Sw*HaCE, HeteroAnalysis indicates a molecular mass of 144.3 kDa, which is close to the theoretical molecular mass expected for a dimer, 149 kDa (Figure 6A and Table 1). For WT *Sw*H-NOX, as either the Fe(II)-unligated or

Table 1. Summary of Sedimentation Equilibrium Results and Controls

protein/protein complex	calculated molecular mass (theoretical molecular mass) (kDa)[f]
HaCE by itself[a,b]	144.3 (149.0, dimer)
HaCE with WT H-NOX Fe(II)−NO[a,c]	197.2 (193.0, 2+2 heterotetramer)
HaCE with WT H-NOX Fe(II)[a,d]	198.0 (193.0, 2+2 heterotetramer)
HaCE with E16K H-NOX Fe(II)−NO[a,c]	76.0 (−)
WT H-NOX Fe(II)−NO[a,c]	75.0 (−)
WT H-NOX Fe(II)−NO[e,c]	23.3 (22.5, monomer)
WT H-NOX Fe(II)[e,d]	23.0 (22.5, monomer)
E16K H-NOX Fe(II)−NO[e,c]	23.8 (22.5, monomer)

[a]The sedimentation equilibrium run was conducted at three rotor speeds calculated for the molecular mass of *Sw*HaCE (74.5 kDa): 9000 rpm (6520g), 14000 rpm (15800g), and 18000 rpm (26100g). [b]The scans for the sedimentation equilibrium runs were collected at 280 nm. [c]The scans for the sedimentation equilibrium runs were collected at 400 nm. [d]The scans for the sedimentation equilibrium runs were collected at 430 nm. [e]The sedimentation equilibrium run was conducted at three rotor speeds calculated for the molecular mass of *Sw*H-NOX (22.5 kDa): 17000 rpm (23300g), 27000 rpm (58700g), and 34000 rpm (93100g). [f]HeteroAnalysis and Sednterp were used to calculate the molecular mass.

Fe(II)−NO complex, our analysis indicated a molecular mass of 23 kDa, which is close to the theoretical molecular mass of 22.5 kDa (Figure S1 of the Supporting Information and Table 1). Thus, WT *Sw*H-NOX alone exists as a monomer and *Sw*HaCE as a dimer.

The molecular mass for the *Sw*H-NOX/*Sw*HaCE complex, which was monitored at 400 nm (to follow heme absorbance), was calculated to be 197.2 kDa when *Sw*H-NOX was run as the Fe(II)−NO complex (Figure 6B and Table 1) and 198.0 kDa when *Sw*H-NOX was run as the Fe(II)-unligated complex (monitored at 430 nm to follow heme absorbance) (Figure S2 of the Supporting Information and Table 1), both of which are close to the theoretical molecular mass of 193 kDa for a heterotetrameric complex of four molecules comprised of two *Sw*HaCE monomers and two *Sw*H-NOX monomers. All of the molecular masses computed from the AUC experiments are within 3% of the theoretical value, which is within the experimental error of the instrument. Therefore, we conclude that *Sw*HaCE and *Sw*H-NOX form a 2:2 heterotetrameric protein complex in solution, regardless of whether NO is bound to *Sw*H-NOX. Because *Sw*H-NOX and *Sw*HaCE are cocistronic, these data support our model in which H-NOX and HaCE likely form a complex upon production in bacterial cells.[24] This is the first H-NOX/HaCE protein complex stoichiometry to have been determined.

The E16K *Sw*H-NOX mutant [as the Fe(II)−NO complex] was analyzed both by itself and as a complex with *Sw*HaCE. The mutant was determined to be a monomer by itself [calculated molecular mass of 23 kDa (Figure S1 of the Supporting Information and Table 1)], similar to WT *Sw*-NOX. The E16K *Sw*H-NOX/*Sw*HaCE protein mixture, followed at the heme absorbance, did not form a complex, as suggested by the calculated molecular mass of 76.5 kDa (Figure S2 of the Supporting Information and Table 1). In support of this, when *Sw*H-NOX was run without *Sw*HaCE at the optimal rotor speeds to analyze the 193 kDa *Sw*H-NOX/*Sw*HaCE complex, rather than the 22.5 kDa *Sw*H-NOX species alone, we
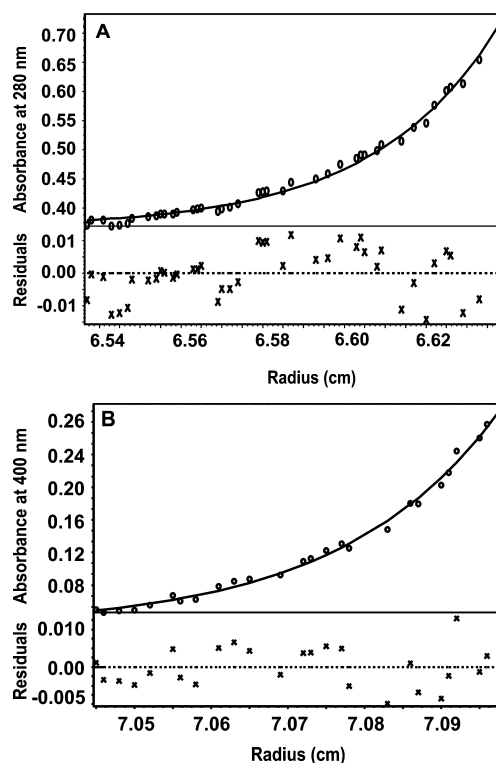

Figure 6. (A) Sedimentation equilibrium experiments with *Sw*HaCE in solution. Using rotor speeds of 9000, 14000, and 18000 rpm (which are equal to 6500g, 15800g, and 26100g, respectively), and following protein at 280 nm, the calculated molecular mass of *Sw*HaCE is 144.3 kDa, indicating a dimer in solution at equilibrium. (B) Sedimentation equilibrium experiment for *Sw*HaCE in solution with the *Sw*H-NOX Fe(II)−NO complex. Using rotor speeds of 9000, 14000, and 18000 rpm (which are equal to 6500g, 15800g, and 26100g, respectively), and following protein complexes at 400 nm, the calculated molecular mass for the complex is 197.2 kDa at equilibrium. This matches the molecular mass expected for a heterotetramer of two *Sw*H-NOX proteins and two *Sw*HaCE proteins. Each experiment was conducted in triplicate.

obtained a calculated molecular mass of 75 kDa (Figure S2 of the Supporting Information and Table 1). The molecular mass of *Sw*H-NOX is not accurately calculated at the rotor speeds used to analyze the *Sw*H-NOX/*Sw*HaCE complex because higher angular velocities are required for lower-molecular mass solutes to balance the sedimentation and diffusion forces within the radius of the centrifuge cell. This result again suggests a loss of *Sw*H-NOX/*Sw*HaCE binding due to this *Sw*H-NOX surface mutation.

Enzyme Assays Confirm the *Sw*H-NOX/*Sw*HaCE Binding Interface. Next we tested the effect of *Sw*H-NOX and *Sw*H-NOX surface mutants on the regulation of *Sw*HaCE activity. We have previously reported that the diguanylate cyclase activity for *Sw*HaCE increases in the presence of the WT *Sw*H-NOX Fe(II)-unligated complex, whereas the phosphodiesterase activity is enhanced in the presence of the WT *Sw*H-NOX Fe(II)−NO complex.[24] In these studies, we used a new reaction end point assay for cyclase activity, based on the detection of phosphate (P_i) in solution with the dye Malachite green.

In a diguanylate cyclase-catalyzed reaction, two molecules of GTP are condensed to generate PP_i (inorganic pyrophosphate) as a byproduct along with cyclic-di-GMP (2GTP → cyclic-di-

GMP + 2PP$_i$).[35] In the presence of the enzyme inorganic pyrophosphatase (IPP), PP$_i$ is hydrolyzed to P$_i$ (inorganic phosphate) in solution (2PP$_i$ → 2P$_i$).[36] Malachite green is a commercially available reagent, which is used to determine the concentration of free P$_i$ in solution.[37] This end point assay can be used to quantify diguanylate cyclase activity by measuring the amount of P$_i$ generated from PP$_i$ produced during the reaction. Because this is an end point assay, the SwHaCE enzyme was boiled before IPP was added to the solution to ensure that IPP does not interfere with the activity of the enzyme. To confirm that IPP is not the rate-limiting enzyme in the reaction, the concentration of IPP was doubled to confirm that the same amount of P$_i$ was generated (Table S2 of the Supporting Information). Because we are detecting the amount of PP$_i$ produced in the reaction, the turnover of cyclic-di-GMP into pGpG by the phosphodiesterase domain of SwHaCE does not affect the measurement. As a control, the amount of P$_i$ generated was determined at various concentrations of SwHaCE (Figure S3 of the Supporting Information). A linear correlation was observed between the enzyme concentration and the amount of P$_i$ produced, confirming that only SwHaCE is the rate-limiting enzyme in the reaction.

This assay was used to determine the concentration of P$_i$ generated during the reaction of SwHaCE with GTP in the presence of the WT, E16K, F17A, and E20K SwH-NOX Fe(II)-unligated complexes. The specific activity values are reported in Figure 7 as concentrations of P$_i$ (micromolar per minute per
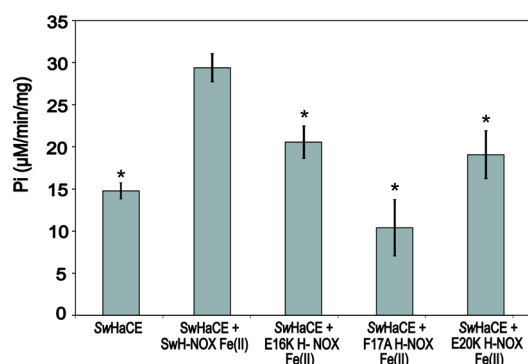

Figure 7. Regulation of SwHaCE diguanylate cyclase activity by SwH-NOX. Addition of 20 µM Fe(II)-unligated complex of SwH-NOX to SwHaCE causes a significant increase in the specific activity of SwHaCE. Addition of any of the Fe(II)-unligated SwH-NOX surface mutants (E16K, F17A, and E20K, all at 20 µM), however, had a weaker effect or no effect on SwHaCE activity, indicating weakened binding to SwHaCE. All assays contained 1 µM SwHaCE and 200 µM GTP as substrate. Error bars represent three independent trials on different days. A Student's p test was conducted to determine significance. Asterisks indicate $p \leq 0.006$. Each data set was compared to the activity of SwHaCE with WT SwH-NOX Fe(II).

milligram). It was observed that the WT SwH-NOX Fe(II)-unligated complex (20 µM) increased the initial velocity of the cyclase activity of SwHaCE (1 µM) by 2-fold in the presence of 200 µM GTP, as expected from our previous work[24] (Figure 7). In general, addition of the SwH-NOX mutants led to a loss of this enhanced effect, indicating a loss of SwH-NOX binding and regulation of SwHaCE cyclase activity. For the E16K and E20K SwH-NOX mutants, the observed initial velocity was lower than that of SwHaCE with WT SwH-NOX but slightly higher than that of the enzyme by itself, indicating some residual binding and regulation by SwH-NOX, but significantly

less than that observed with WT SwH-NOX. For F17A SwH-NOX, we observed the same initial velocity as SwHaCE without SwH-NOX. These data, like all of the experiments described above, also indicate that SwH-NOX/SwHaCE binding has been disrupted by the surface mutations and support our conclusion that SwH-NOX binds to SwHaCE, at least in part, using the N-terminal helical region of H-NOX.

■ DISCUSSION

The spatiotemporal regulation of intracellular cyclic-di-GMP is central to many important cellular processes like virulence, biofilm formation, quorum sensing, motility, and cell division.[38,39] Diguanylate cyclase and phosphodiesterase enzymes, which maintain the intracellular pool of cyclic-di-GMP, are usually found to be associated with regulatory domains and/or proteins that modulate their activity. However, very few of these enzymes have been characterized with their regulatory partner protein.

NO has been shown to play an important role in bacterial signaling, and recent studies have indicated that low concentrations of NO disperse biofilms in bacteria through the regulation of cyclic-di-GMP concentrations.[40] We have previously reported that NO disperses biofilms in the marine, bioluminescent, biofilm-dwelling bacterium S. woodyi through H-NOX by regulating the production of cyclic-di-GMP by HaCE.[24] It was shown that SwH-NOX and NO differentially modulate the enzymatic activities of both the diguanylate cyclase and phosphodiesterase domains of SwHaCE. These results necessitate a model in which H-NOX and HaCE are associated in a manner that is independent of the ligation state of H-NOX. Data presented in this study confirm that SwH-NOX and SwHaCE form a complex independent of the ligation state of H-NOX.

This study investigates the structural and biophysical details of the association between SwH-NOX and SwHaCE. We have used NMR chemical shift perturbation analysis along with peak assignments for SwH-NOX to identify the critical H-NOX surface residues that are involved in binding to SwHaCE. The tremendous change in the chemical environment of a patch of N-terminal residues, including residues E16, F17, and E20, indicates a binding region for SwHaCE on SwH-NOX (Figure 3A,B). We also identified other residues (approximately six or seven) with significant chemical shift perturbations upon binding to SwHaCE that are spread out on other parts of SwH-NOX. These chemical shift perturbations may indicate additional binding surface area or, alternatively, a conformational rearrangement of SwH-NOX that is triggered upon binding to SwHaCE.

To determine the role of identified SwH-NOX N-terminal amino acids (E16, F17, and E20) in binding SwHaCE, we made mutants of each and investigated the effect of mutation in several binding and enzymatic assays. Fluorescence binding assays indicate a significant loss of binding (Figure 5) and alteration of enzyme regulation (Figure 7) for individual mutants of these surface residues (E16, F17, and E20). Hence, we can conclude that these residues mediate interaction of SwH-NOX with SwHaCE. Sedimentation equilibrium experiments reveal the WT SwH-NOX/SwHaCE protein complex to be a heterotetramer (Figure 6B), in both the Fe(II)-unligated and Fe(II)−NO-bound states, whereas SwH-NOX alone and all the surface mutants in the presence of SwHaCE were determined to be monomeric in solution.

On the basis of our results, we developed a model for the SwH-NOX/SwHaCE protein complex. Because SwH-NOX and SwHaCE are cocistronic,[24] we hypothesize that they are expressed together in the cell and always associate to form this heterotetrameric complex. This association likely occurs via dimerization of SwHaCE, followed by binding of two molecules of SwH-NOX to the SwHaCE dimer, as illustrated in Figure 8.
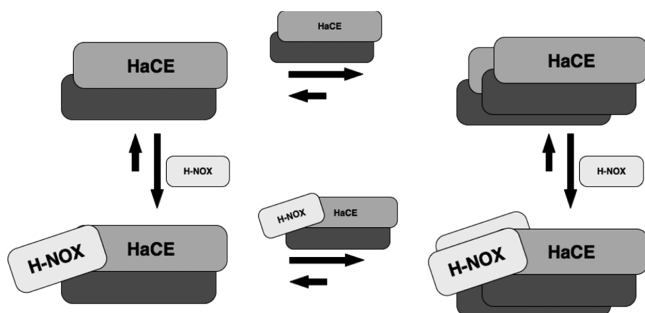

Figure 8. Possible mechanism of formation of the complex between SwHaCE and SwH-NOX. Monomeric SwHaCE is likely in equilibrium with dimeric SwHaCE, with the equilibrium lying toward the dimer. Monomeric or dimeric SwHaCE may associate with one or two molecules of SwH-NOX, respectively. The most abundant species at equilibrium is the heterotetrameric complex (2:2), containing two molecules each of SwHaCE and SwH-NOX.

Upon expression, presumably, SwH-NOX is in the Fe(II)-unligated state, and hence, the cyclase activity of SwHaCE is enhanced to generate more cyclic-di-GMP. When the signal (NO) binds, there must be a change in the conformation of the heterotetrameric protein complex, leading to a change in the activity of SwHaCE that results in less cyclic-di-GMP produced, ultimately causing biofilm dispersal. If monomeric SwHaCE also binds SwH-NOX, there may be a complex equilibrium involving dimerization of SwHaCE, monomeric association of the SwH-NOX/SwHaCE complex, and two monomers of SwH-NOX binding to the SwHaCE dimer to form the final heterotetrameric species. However, sedimentation equilibrium cannot be used to determine the ratio of these species in solution.

Furthermore, the data presented here indicate that N-terminal helices αA–αC mediate binding to SwHaCE. This result is supported by several previous studies that also point to the role of the N-terminal helices in transmitting the signal of NO binding to H-NOX partner proteins. In crystal structures of the H-NOX domain from *Nostoc punctiforme*,[41] the N-terminal helices have been shown to be maximally displaced upon binding of the signaling ligands NO and CO, suggesting that movement in helices αA–αC constitutes part of the signal transfer mechanism. Furthermore, a recent study from the Marletta lab describes the important higher-order interactions in sGC, elucidating the mechanism of NO-regulated stimulation of activity.[42] They found that in the N-terminal region of sGC, H-NOX participates in the signal transfer mechanism by binding to the PAS domain. Mutational studies confirm that NO binding triggers these local interactions, leading to global conformational changes, ultimately increasing activity.

Further evidence that the N-terminal helices of H-NOX are important for interaction with partner proteins and signal propagation comes from studies of the structure of the heme cofactor of H-NOX. The heme unit in H-NOX is highly distorted from planarity,[43] but structural studies have indicated that mutation of a conserved proline residue in the proximal heme pocket causes substantial heme flattening.[44] The conformational change caused by heme flattening propagates to the surface of H-NOX, causing a shift in the position of the N-terminal helices. We have shown in SwH-NOX that the heme-flattened mutant affects SwHaCE activity exactly the same as binding of NO to WT SwH-NOX,[45] indicating heme flattening causes a structural change similar to that of binding of the SwH-NOX/SwHaCE complex to NO. These data suggest that transmission of the NO signal involves the N-terminal helices, which is highly supportive of our results reported here, indicating the N-terminal helices are involved in binding HaCE, which is required for translation of NO binding to the enzymatic active sites.

Taken together, there is strong evidence that ligand binding events in bacterial H-NOX domains cause conformational changes that are relayed to the N-terminal helices, which serve as a binding site for interaction with partner enzymes such as HaCEs or HahKs (H-NOX-associated histidine kinases), ultimately resulting in functional changes within the cell.

In conclusion, NO and cyclic-di-GMP are becoming increasingly important as signaling molecules that direct bacteria on how to make the choice between motile and sessile lifestyles. This study is the first of its kind that provides a structural understanding of how a bacterial NO-sensing protein, H-NOX, can regulate its associated enzyme activity (HaCE and HahK), to control the downstream functions such as biofilm formation. Such studies improve our understanding of how small molecule signaling regulates downstream functions and how enzymes that regulate the cyclic-di-GMP concentration in the cell are functionally regulated by a signal-sensing protein.

■ ASSOCIATED CONTENT

Ⓢ Supporting Information

Soret band maxima and NO dissociation rate constants for Fe(II), Fe(II)−NO, and Fe(II)−CO species for WT, E16K, F17A, and E20K SwH-NOX; a standard curve for PP$_i$ concentration; data showing that generation of P$_i$ from PP$_i$ by IPP is not the rate-limiting step in our kinetic assays; a plot of the amount of P$_i$ generated during the diguanylate cyclase reaction of SwHaCE using GTP as a substrate at different SwHaCE concentrations; and sedimentation equilibrium experiments with WT SwH-NOX, E16K SwH-NOX, and the E16K SwH-NOX/SwHaCE mixture at different speeds. This material is available free of charge via the Internet at http://pubs.acs.org.

■ AUTHOR INFORMATION

Corresponding Author
*Department of Chemistry, Stony Brook University, Stony Brook, NY 11790. E-mail: elizabeth.boon@stonybrook.edu. Telephone: (631) 632-7945. Fax: (631) 632-7960.

Notes
The authors declare no competing financial interest.

■ ABBREVIATIONS

NO, nitric oxide; H-NOX, heme-nitric oxide/oxygen-binding; HaCE, H-NOX-associated cyclic-di-GMP processing enzyme; DGC, diguanylate cyclase; PDE, phosphodiesterase; GTP, guanosine triphosphate; c-di-GMP or cyclic-di-GMP, bis-(3′−5′)-cyclic dimeric guanosine monophosphate; pGpG, 5′-phosphoguanylyl-(3′−5′)-guanosine; Sw, $S.$ $woodyi$; GGDEF, conserved amino acids in the catalytic sites of diguanylate cyclases (the domain containing these conserved residues is often termed a GGDEF domain); EAL, conserved amino acids in the catalytic site of phosphodiesterases (the domain containing these conserved residues is often termed an EAL domain); sGC, soluble guanylate cyclase (a eukaryotic H-NOX domain-containing protein); SwHaCE, wild-type $S.$ $woodyi$ diguanylate cyclase/phosphodiesterase protein used in this study; SwH-NOX, wild-type H-NOX protein used in this study; IPTG, isopropyl β-D-1-thiogalactopyranoside; OD, optical density; Tris, tris(hydroxymethyl)aminomethane; PMSF, phenylmethanesulfonyl fluoride; BME, β-mercaptoethanol; NMR, nuclear paramagnetic resonance spectroscopy; BSA, bovine serum albumin; TROSY, transverse relaxation-optimized spectroscopy; HSQC, heteronuclear single-quantum coherence; HNCO, HNCACB, CBCACONH, and HNCA, triple-resonance nuclear magnetic resonance spectroscopy to assign protein backbone atoms; AUC, analytical ultracentrifugation; MG, Malachite green; IPP, inorganic pyrophosphatase; PP_i, inorganic pyrophosphate.

■ REFERENCES

(1) Galperin, M. Y. (2004) Bacterial signal transduction network in a genomic perspective. *Environ. Microbiol. 6* (6), 552−567.

(2) Karatan, E., and Watnick, P. (2009) Signals, regulatory networks, and materials that build and break bacterial biofilms. *Microbiol. Mol. Biol. Rev. 73* (2), 310−347.

(3) D'Argenio, D. A., and Miller, S. I. (2004) Cyclic-di-GMP as a bacterial second messenger. *Microbiology 150* (Part 8), 2497−2502.

(4) Jenal, U. (2004) Cyclic di-guanosine-monophosphate comes of age: A novel secondary messenger involved in modulating cell surface structures in bacteria. *Curr. Opin. Microbiol. 7* (2), 185−191.

(5) Jenal, U., and Malone, J. (2006) Mechanisms of cyclic-di-GMP signaling in bacteria. *Annu. Rev. Genet. 40*, 385−407.

(6) Cotter, P. A., and Stibitz, S. (2007) C-di-GMP-mediated regulation of virulence and biofilm formation. *Curr. Opin. Microbiol. 10* (1), 17−23.

(7) Tamayo, R., Pratt, J. T., and Camilli, A. (2007) Roles of cyclic diguanylate in the regulation of bacterial pathogenesis. *Annu. Rev. Microbiol. 61*, 131−148.

(8) Hengge, R. (2009) Principles of c-di-GMP signalling in bacteria. *Nat. Rev. Microbiol. 7* (4), 263−273.

(9) Aldridge, P., Paul, R., Patrick, G., Rainey, P., and Jenal, U. (2003) Role of the GGDEF regulator PleD in polar development of *Caulobacter crescentus. Mol. Microbiol. 47* (6), 1695−1708.

(10) Iyer, L., Anantharaman, V., and Aravind, L. (2003) Ancient conserved domains shared by animal soluble guanylyl cyclases and bacterial signaling proteins. *BMC Genomics 4* (1), 1−8.

(11) Ryjenkov, D. A., Tarutina, M., Moskvin, O. V., and Gomelsky, M. (2005) Cyclic diguanylate is a ubiquitous signaling molecule in bacteria: Insights into biochemistry of the GGDEF protein domain. *J. Bacteriol. 187* (5), 1792−1808.

(12) Christen, M., Christen, B., Folcher, M., Schauerte, A., and Jenal, U. (2005) Identification and characterization of a cyclic di-GMP-specific phosphodiesterase and its allosteric control by GTP. *J. Biol. Chem. 280* (35), 30829−30837.

(13) Schmidt, A. J., Ryjenkov, D. A., and Gomelsky, M. (2005) The ubiquitous protein domain EAL is a cyclic diguanylate-specific phosphodiesterase: Enzymatically active and inactive EAL domains. *J. Bacteriol. 187* (14), 4774−4781.

(14) Ryan, R. P., Fouhy, Y., Lucey, J. F., Crossman, L. C., Spiro, S., He, Y. W., Zhang, L. H., Heeb, S., Camara, M., Williams, P., and Dow, J. M. (2006) Cell-cell signaling in *Xanthomonas campestris* involves an HD-GYP domain protein that functions in cyclic di-GMP turnover. *Proc. Natl. Acad. Sci. U.S.A. 103* (17), 6712−6717.

(15) Denninger, J. W., and Marletta, M. A. (1999) Guanylate cyclase and the NO/cGMP signaling pathway. *Biochim. Biophys. Acta 1411*, 334−350.

(16) Boon, E. M., Huang, S. H., and Marletta, M. A. (2005) A molecular basis for NO selectivity in soluble guanylate cyclase. *Nat. Chem. Biol. 1* (1), 53−59.

(17) Barraud, N., Schleheck, D., Klebensberger, J., Webb, J. S., Hassett, D. J., Rice, S. A., and Kjelleberg, S. (2009) Nitric oxide signaling in *Pseudomonas aeruginosa* biofilms mediates phosphodiesterase activity, decreased cyclic di-GMP levels, and enhanced dispersal. *J. Bacteriol. 191* (23), 7333−7342.

(18) An, S., Wu, J., and Zhang, L. H. (2010) Modulation of *Pseudomonas aeruginosa* biofilm dispersal by a cyclic-di-GMP phosphodiesterase with a putative hypoxia-sensing domain. *Appl. Environ. Microbiol. 76* (24), 8160−8173.

(19) Yukl, E. T., Ioanoviciu, A., Sivaramakrishnan, S., Nakano, M. M., Ortiz de Montellano, P. R., and Moenne-Loccoz, P. (2011) Nitric oxide dioxygenation reaction in DevS and the initial response to nitric oxide in *Mycobacterium tuberculosis. Biochemistry 50* (6), 1023−1028.

(20) Boon, E. M., and Marletta, M. A. (2005) Ligand discrimination in soluble guanylate cyclase and the H-NOX family of heme sensor proteins. *Curr. Opin. Chem. Biol. 9* (5), 441−446.

(21) Arora, D. P., and Boon, E. M. (2012) Nitric oxide regulated two-component signaling in *Pseudoalteromonas atlantica. Biochem. Biophys. Res. Commun. 421* (3), 521−526.

(22) Liu, N., Pak, T., and Boon, E. M. (2010) Characterization of a diguanylate cyclase from *Shewanella woodyi* with cyclase and phosphodiesterase activities. *Mol. BioSyst. 6* (9), 1561−1564.

(23) Carlson, H. K., Vance, R. E., and Marletta, M. A. (2010) H-NOX regulation of c-di-GMP metabolism and biofilm formation in *Legionella pneumophila. Mol. Microbiol. 77* (4), 930−942.

(24) Liu, N., Xu, Y., Hossain, S., Huang, N., Coursolle, D., Gralnick, J. A., and Boon, E. M. (2010) Nitric oxide regulation of cyclic di-GMP synthesis and hydrolysis in *Shewanella woodyi. Biochemistry 51* (10), 2087−2099.

(25) Bradford, M. M. (1976) A rapid and sensitive method for the quantitation of microgram quantities of protein utilizing the principle of protein-dye binding. *Anal. Biochem. 72*, 248−254.

(26) Erbil, W. K., Price, M. S., Wemmer, D. E., and Marletta, M. A. (2009) A structural basis for H-NOX signaling in *Shewanella oneidensis* by trapping a histidine kinase inhibitory conformation. *Proc. Natl. Acad. Sci. U.S.A. 106* (47), 19753−19760.

(27) Delaglio, F., and Bax, A. (1995) NMRPipe: A multidimensional spectral processing system based on UNIX pipes. *J. Biomol. NMR 6*, 277−293.

(28) Goddard, T. D., and Kneller, D. G. (2008) *SPARKY 3*, University of Calfornia, San Francisco.

(29) Schuck, P. (2000) Size-Distribution Analysis of Macromolecules by Sedimentation Velocity Ultracentrifugation and Lamm Equation Modeling. *Biophys. J. 78*, 1606−1619.

(30) Boon, E. M., Davis, J. H., Tran, R., Karow, D. S., Huang, S. H., Pan, D., Miazgowicz, M. M., and Marletta, M. A. (2006) Nitric oxide binding to prokaryotic homologs of the soluble guanylate cyclase β1 H-NOX domain. *J. Biol. Chem. 281* (31), 21892−21902.

(31) Cole, J. L., Lary, J. W., Moody, T., and Laue, T. M. (2008) Analytical Ultracentrifugation: Sedimentation Velocity and Sedimentation Equilibrium. *Methods Cell Biol. 84*, 143−179.

(32) Malone, J. G., Williams, R., Christen, M., Jenla, U., Spiers, A. J., and Rainey, P. B. (2007) The structure-function relationship of WspR, a *Pseudomonas fluorescens* response regulator with a GGDEF output domain. *Microbiology 153* (Part 4), 980−994.

(33) Paul, R., Abel, S., Wassmann, P., Beck, A., Heerklotz, H., and Jenal, U. (2007) Activation of the Diguanylate Cyclase PleD by Phosphorylation-mediated Dimerization. *J. Biol. Chem. 282* (40), 29170−29177.

(34) De, N., Pirruccello, M., Krasteva, P. V., Bae, N., Raghavan, R. V., and Sondermann, H. (2008) Phosphorylation-independent regulation of the diguanylate cyclase WspR. *PLoS Biol. 6* (3), e67.

(35) Chan, C., Paul, R., Samoray, D., Amiot, N. C., Giese, B., Jenal, U., and Schirmer, T. (2004) Structural basis of activity and allosteric control of diguanylate cyclase. *Proc. Natl. Acad. Sci. U.S.A. 101* (49), 17084−17089.

(36) Upson, R. H., Haugland, R. P., Malekzadeh, M. N., and Haugland, R. P. (1996) A Spectrophotometric Method to Measure Enzymatic Activity in Reactions That Generate Inorganic Pyrophosphate. *Anal. Biochem. 243* (1), 41−45.

(37) Carter, S. G., and Karl, D. W. (1982) Inorganic phosphate assay with malachite green: An improvement and evaluation. *J. Biochem. Biophys. Methods 7* (1), 7−13.

(38) Mills, E., Pultz, I. S., Kulasekara, H. D., and Miller, S. I. (2011) The bacterial second messenger c-di-GMP: Mechanisms of signalling. *Cell. Microbiol. 13* (8), 1122−1129.

(39) Krasteva, P. V., Giglio, K. M., and Sondermann, H. (2012) Sensing the messenger: The diverse ways that bacteria signal through c-di-GMP. *Protein Sci. 21* (7), 929−948.

(40) McDougald, D., Rice, S. A., Barraud, N., Steinberg, P. D., and Kjelleberg, S. (2012) Should we stay or should we go: Mechanisms and ecological consequences for biofilm dispersal. *Nat. Rev. Microbiol. 10* (1), 39−50.

(41) Ma, X., Sayed, N., Beuve, A., and van den Akker, F. (2007) NO and CO differentially activate soluble guanylyl cyclase via a heme pivot-bend mechanism. *EMBO J. 26*, 578−588.

(42) Underbakke, E. S., Iavarone, A. T., and Marletta, M. A. (2013) Higher-order interactions bridge the nitric oxide receptor and catalytic domains of soluble guanylate cyclase. *Proc. Natl. Acad. Sci. U.S.A. 110* (17), 6777−6782.

(43) Pellicena, P., Karow, D. S., Boon, E. M., Marletta, M. A., and Kuriyan, J. (2004) Crystal structure of an oxygen-binding heme domain related to soluble guanylate cyclases. *Proc. Natl. Acad. Sci. U.S.A. 101* (35), 12854−12859.

(44) Olea, C., Boon, E. M., Pellicna, P., Kuriyan, J., and Marletta, M. A. (2008) Probing the function of heme distortion in the H-NOX family. *ACS Chem. Biol. 3* (11), 703−710.

(45) Muralidharan, S., and Boon, E. M. (2012) Heme flattening is sufficient for signal transduction in the H-NOX family. *J. Am. Chem. Soc. 134* (4), 2044−2046.